Molecular dynamics simulation of the six- to four-coordinate pressure-driven transition in *MX* nanocrystals: Mechanistic consequences of Σ_3 grain boundaries in the high-pressure starting structure

Benjamin J. Morgan*
School of Chemistry, Trinity College, University of Dublin, Dublin 2, Ireland
(Received 26 April 2008; published 15 July 2008)

Constant-pressure molecular dynamics has been used to simulate the six- to four-coordinate downstroke pressure-driven phase transition in B1 nanocrystals. The nanocrystals considered have previously been formed in upstroke B3→B1 simulations, giving them an amorphous surface region and interior Σ_3 grain boundaries. Nucleation occurs in the interior of the crystal, with multiple nucleation events observed along grain boundaries, in contrast to previous decompression simulations of single-domain nanocrystals with crystallographically well-defined surfaces. Competing mechanisms give rise to B3, B4, and d-BCT domains in the product structures. Four distinct mechanisms are observed, including two B4↔B1 mechanisms. The $\mathrm{B4}\overset{\mathrm{I}}{\leftrightarrow}\mathrm{B1}$ mechanism is the same as seen in previous simulations of single-domain nanocrystalline and bulk systems, while the observed $\mathrm{B3}\overset{\mathrm{II}}{\leftrightarrow}\mathrm{B1}$ and B4↔B1 display a $[111]_{B3}\leftrightarrow[100]_{B1}$ correspondence, in agreement with experimental observations of repeatedly transformed CdSe nanocrystals; both of which are different to those seen in previous upstroke simulations. The interaction between these competing mechanisms determines the domain structure of the product nanocrystals.

DOI: 10.1103/PhysRevB.78.024110 PACS number(s): 81.30.Hd, 61.46.Df

I. INTRODUCTION

III–V and II–VI semiconductors are compounds of broad technological importance. Under ambient conditions the directional bonding of these materials gives tetrahedrally bonded open structures; typically zinc-blende (B3) or wurtzite (B4). Upon the application of pressure they undergo phase transitions to denser six-coordinate structures, particularly rock salt (B1).[1–4] Copper and silver halides and more ionic materials, such as ZnO, also exhibit these same pressure-driven transitions.[5]

Nanocrystalline samples of these materials display the same phase behavior, and a substantial particle size effect on the thermodynamics and kinetics of the transition has been demonstrated.[6] In crystalline CdS, the pressure required to induce a transformation from a four- to six-coordinate phase increases from 2 to 9 GPa as the particle size is decreased.[7] Many other thermodynamic, mechanical, and electronic properties are also strongly size dependent.[8] For example, as the size of CdS crystals is reduced, the band gap can be selectively varied between 2.5 and 4 eV.[9] Thus nanoscale synthesis offers a means of producing materials with properties tailored to specific applications. Through manipulation of surface energies, it is possible to control the relative stability of different polymorphs,[10–12] potentially opening routes to metastable high-pressure phases with novel properties.[5] The development of such synthetic procedures requires an understanding of the pathways between competing polymorphs, and how these pathways are modified by the finite size of nanoscale systems, in particular by the presence of specific geometric features, such as nonequilibrium surface distributions.

There has been much theoretical work investigating possible pathways for the transitions between four- and six-coordinate systems as seen in pressure-driven phase transitions. Molecular dynamics (MD) studies of bulk systems[13–15] and *ab initio* studies of proposed intermediates[4,16–21] have indicated a number of closely related mechanisms. For all these cases the general local mechanism can be described by two motions: the closing up of hexagons oriented in the $[0001]_{B4}$ plane to form 2×3 pairs of square rings, and the flattening of staggered *ab* planes to form $[001]_{B1}$ planes. Together these are analogous to a reverse Peierls-type distortion.[22,23] Saitta and Decremps[24] have shown that the differences between specific mechanisms depend upon the order in which these orthogonal movements occur. Experimental support for this general mechanism comes from shock experiments performed on CdS crystals[25] and x-ray diffraction data.[26] The closing of hexagonal rings causes groups of atoms lying along $[11\bar{2}0]$ planes to move past each other, and different global mechanisms have been identified, in which this pattern of relative motion is parallel or antiparallel on a range of length scales.[14,27] The precise pathway, however, is expected to be material dependent, and may vary with morphology since this will affect nucleation barriers and surface energy contributions to the free energies of the competing phases.

Molecular dynamics simulations of the compression of B4 nanocrystals have shown that the same general mechanism is followed,[28–33] proceeding via surface nucleation and subsequent domain growth. This process of nucleation and growth has also been observed in bulk simulations of CdSe by Zahn *et al.*[15]

The B3→B1 transition mechanism has also been studied, using molecular dynamics in bulk[34,35] and nanocrystalline[36–38] systems. In both cases the transition was found to proceed via a tetragonal distortion involving a compression of the $[001]_{B3}$ vector to a diatomic-β-tin-like structure, followed by a concerted motion of the cation sublattice along the $[001]_{B3}$ direction, and a synchronous movement of

alternating layers of the anion sublattice in opposite $[100]_{B1}$ and $[\bar{1}00]_{B1}$ directions. Miao and Lambrecht[39] have shown that this tetragonal intermediate is common to a broad range of compounds. However an extensive first-principles examination of 925 pathways by Hatch *et al.*[40] concluded that those pathways with the lowest energy barriers consist of $(111)_{B3}$ layers sliding over one another. These two proposed B3→B1 mechanisms (via tetragonal distortion and via $(111)_{B3}$ bilayer sliding) have the same relationship between the initial and final crystal lattices—$[111]_{B3} \leftrightarrow [111]_{B1}$—but have different transition states.

Downstroke six- to four-coordinate transitions have received less attention than their upstroke counterparts. While identical pathways are obvious candidates for both directions of phase change, it is possible that the transition behavior is asymmetric. Cycled transitions in nanocrystals display a significant hysteresis, and relative barrier heights on the relevant potential-energy surface might be pressure dependent, particularly if alternative transition states are different distances along their respective pathways, and hence have different associated activation volumes.[41] Furthermore, in nanoscale systems, modification of the surface energy through surface annealing[5,42] or solvent effects[10,11,43,44] might be exploited to modify both the free-energy difference between high- and low-pressure phases, and hence the thermodynamic driving force, and the barrier heights for specific pathways, allowing kinetic control over the mechanism.

B1 nanocrystals initially formed from simulated B4→B1 upstroke transitions to give a hexagonal prismatic morphology, and B1 nanocrystals with a cubic morphology that represent an optimally equilibrated high-pressure structure, are predicted in simulations to transform at different pressures and by different mechanisms. This demonstrates that very different behavior can occur if low energy pathways are frustrated. Simulations of the downstroke transitions thus not only attempt to describe the behavior of high-pressure nanocrystals formed with particular morphological features, but also provide a means of observing potential alternative four- to six-coordinate pathways, which could play a role in the transformation of real systems.

An experimental study of particular interest is that of Wickham *et al.*,[45] who reported that mixed B3/B4 CdSe nanocrystals undergo repeatable transition cycles on the application and removal of pressure. The samples were single-domain nanocrystals with the same *c* close-packed orientation throughout. The B3 and B4 subregions are the results of variation in the stacking sequence in individual nanoparticles. The recovery of single-domain mixed B3/B4 nanocrystals, after complete compression–decompression cycles, indicates a B1→B3 transition having taken place. Such a mechanism has not been identified in previous simulations. Furthermore, the B4→B1 mechanism seen for facetted crystals and in the bulk is incompatible with the lattice orientation relationship inferred by Wickham *et al.* from diffraction data, which indicates a correspondence between the $[111]_{B3}/[0001]_{B4}$ and $[111]_{B1}$ directions. However, it has been noted previously[13] that the presence of stacking faults in B3 systems (of which B4 is an extreme example) prevents the formation of the layers of distorted tetrahedra, which characterizes the intermediate structure in the previously seen B3→B1 transition mechanism, and this may be the reason for the differences between this experimental data and the previous simulations of single-domain nanocrystals. Understanding the phase behavior of mixed B3/B4 nanostructures is of topical interest, since specific polytypes of AgI with structures equivalent to periodic stacking faults have recently been found to display a huge room-temperature ionic conductivity, and a large hysteresis with respect to the high-temperature α-AgI phase; both of which have been attributed to the large disorder of the Ag lattice, and which suggests potential applications in solid-state battery technologies.[46]

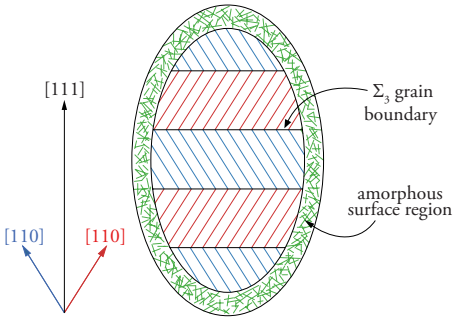

FIG. 1. (Color online) Schematic of the interior of a multidomain high-pressure B1-starting nanocrystal; previously formed by compression of a single-domain B3 nanocrystal (Ref. 37).

This paper describes the reverse six- to four-coordinate transition that B3→B1 nanocrystals undergo as the applied pressure is decreased. The nucleation process for any transition in these clusters will necessarily be different from that seen in previous simulations[42] for nanocrystals with well-defined $\{001\}_{B1}$ and $\{110\}_{B1}$ surfaces. The presence of Σ_3 grain boundaries might also affect the behavior of these nanocrystals, since these were not present in previously modeled B4↔B1 transitions, and are likely to affect the coherence of any reverse reaction. B1 nanocrystals formed through the compression of B3 clusters have strikingly different morphologies to those produced from compression of B4 clusters, and as such are expected to display different downstroke behaviors. The starting high-pressure configuration is illustrated schematically in Fig. 1, which shows a slice through the center of such a nanocrystal. The interior is formed from multiple B1 domains that meet at a series of symmetric Σ_3 grain boundaries. The domains are oriented such that the local $[110]_{B1}$ direction is 30° from the long axis of the nanocrystal with adjacent domains having alternating left- and right-handed tilts. The surface region of these systems is noncrystalline. It is constructed from a disordered hexagonal net similar to that seen at the surface of "bubble" and "onion" clusters observed in smaller systems.[47,48] This four-coordinate region is low in energy and can accommodate distortions during relaxation with ease. This different high-pressure morphology significantly changes the nature of the downstroke transition. Multiple nucleation events are observed, and competing local mechanisms give rise to a mix of structures in the product crystallite. This echoes the recovery of mixed B3/B4 nanocrystals in the pressure cycling ex-

periments of Wickham *et al.*,[45] and provides a further example of how the presence of specific surface- or grain-boundary structures can influence the adopted mechanisms and product geometries.

Several simulation trajectories have been calculated with the starting configurations having undergone thermal equilibration for different lengths of time to give thermally uncorrelated starting structures. The general features observed in the downstroke transition described in Sec. III A are the same for all these trajectories. However, different thermal histories result in variation in the nucleation events and the subsequent competition between the observed mechanisms, producing low-pressure particles with quantitatively very different structures. These different processes are discussed in Sec. III D with illustrative examples used from suitable trajectories.

II. METHODOLOGY

The simulation methodology employed here is the same as for previous calculations of this type.[29,37,42] High-pressure nanocrystals obtained from previous B3→B1 compression simulations[37] are embedded within a binary Lennard–Jones-type fluid for which the potential parameters have been chosen to frustrate vitrification at high pressures. This fluid is used as a pressure-transmission medium, with the external pressure controlled by varying the volume of the simulation cell. The fluid—crystal interactions are described using the same repulsive Lennard–Jones-type function, to produce a compression that is isotropic with respect to surface termination and crystal orientation. After ensuring the system had been thermally equilibrated at a pressure of 14 GPa (the upstroke transitions were observed at pressures of 8.8–10.5 GPa), further molecular dynamics simulations were run, in which the pressure was gradually decreased at a periodic rate of 0.074 GPa every 12 ps using the thermostatted/barostatted MD algorithm due to Martyna *et al.*[49] with a thermostat temperature of 500 K. This is a rapid rate of pressure variation, especially compared with experimental rates but is slow enough that thermal and hydrostatic equilibrium are reached before each successive pressure decrease. The interaction potential for the nanocrystal is a simple ionic model that has a B4 ground-state structure with a B3 phase at a slightly higher energy.[35] The zero-temperature bulk transition pressures between these tetrahedral phases and B1 are 5.7 GPa and 4.8 GPa, respectively. The focus herein is on the structural changes in the interior of the crystal where (locally at least) well-defined crystalline structures are observed in both the initial and final systems.

III. RESULTS

A. Observation of the transition

To examine the underlying structural changes that occur during the simulation, without having these obscured by vibrational motion, geometric configurations were periodically sampled from the simulation trajectory. Keeping the Lennard–Jones fluid fixed, the nanocrystal ions were then relaxed by performing a few steps of a conjugate gradient minimization routine until the potential energy had been decreased by $\frac{3}{2}kT$; an amount equal to the harmonic vibrational contribution to the potential energy. These partially-quenched structures were used for all subsequent analysis.

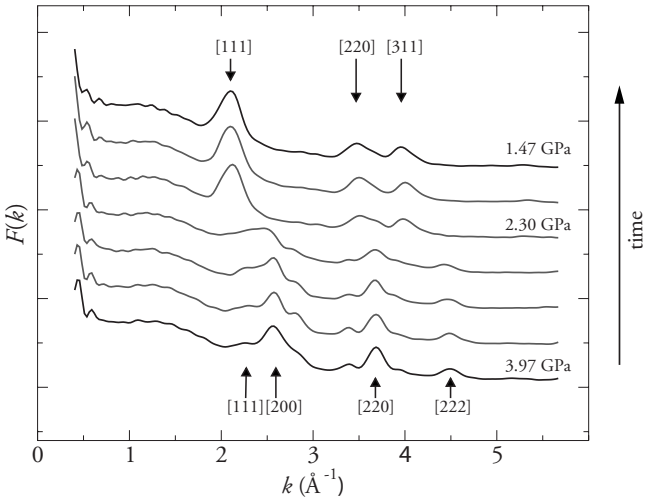

FIG. 2. Calculated diffraction patterns as the pressure applied to a 3246 ion B1 nanocrystal is reduced from 3.97 to 1.47 GPa.

Figure 2 shows calculated diffraction patterns from a 3246 ion nanocrystal as the applied pressure was reduced from 3.97 to 1.47 GPa; a duration of 402 ps. The bottom-most curve, corresponding to a pressure of 3.97 GPa, indexes to a B1 structure, although the peaks are significantly broadened reflecting the multigranular nature of the structure. The broad peak near 1.2 Å^{-1} in the high-pressure patterns corresponds to ordering on a length scale of 5.6 Å. This is the same distance as between the Σ_3 grain boundaries in the high-pressure B1 phase. At a pressure of ~2.3 GPa, the pattern changes indicating a change of structure. This pattern still shows broadened peaks indicating that the multigranular nature of the particle is preserved. The broad peak at low k persists throughout the transition, suggesting there are structural features on this length scale in the product low-pressure nanocrystal. Because of the broadening of the peaks, it is difficult to definitively assign the final pattern to either the B3 or B4 structure. With this resolution, the majority of the peaks for the two structures would appear at the same value of k, although there is a suggestion of a $[102]_{B4}$ peak at ≈ 2.8 Å^{-1}, which would be absent for a pure B3 system.

Figure 3 shows the ion–ion potential energy, $U_{\text{ion-ion}}$, and number of octahedrally coordinated cations $n(O_h)$ for the same nanocrystal as a function of time throughout the same period of the simulation. As the pressure is reduced from 3.97 GPa, $U_{\text{ion-ion}}$ slowly decreases before starting to drop more rapidly after ~225 ps. This decrease in energy slows at around 260 ps but continues at this slower rate until the end of the simulation is reached after 402 ps. The number of octahedrally coordinated cations closely mirrors the behavior of the internal energy. At the start of the simulation, there are approximately 260 such ions. Though the interior of the nanocrystal still appears rock-salt-like under these conditions, this is a small proportion of the total of 1623 cations. This number of cations in octahedral coordination environ-

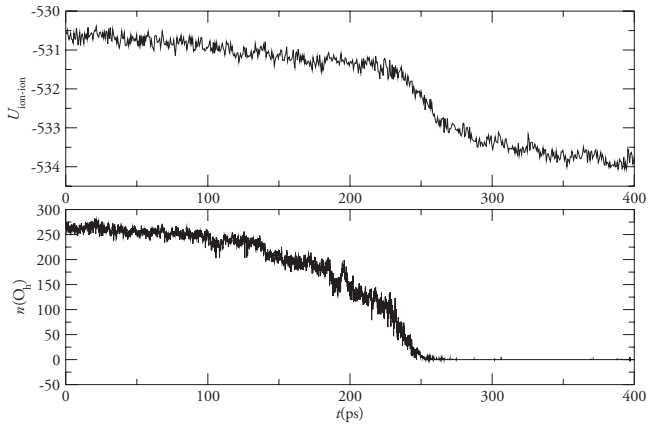

FIG. 3. Ion–ion potential energy and the number of octahedrally coordinated cations during a six- to four-coordinate transformation of a 3246 ion nanocrystal.

ments falls slowly throughout the first portion of the simulation until ~190 ps when it has dropped to around 175. After this the decrease becomes more rapid, mirroring the behavior of the ion-ion potential energy, and by 260 ps $n(O_h)$ has dropped to zero.

B. The formation of a multi-grained product

Figure 4 shows a series of molecular dynamics snapshots of a slice through the interior of the nanocrystal as the external pressure is reduced. This slice has been chosen so that a B1 (110) plane is exposed; the Σ_3 grain boundaries produced during the previous B3→B1 transition are clearly visible, and the $[111]_{B1}$ direction is oriented toward the top of the page. The majority of the interior appears to have the rock-salt structure, yet even at the start of the simulation a row of six-membered rings can be seen near the bottom of the nanocrystal.

As the pressure is decreased, the four-membered rings of the rock-salt structure begin to open up into six-membered rings, suggesting similar processes occurring to those seen in the B1→B4 transition that occurs on depressurization of the single-domain B1 nanocrystals.[42] This first happens along the Σ_3 grain boundaries, and has been highlighted by the arrows in the panels at 164 and 224 ps. After 278 ps, nearly the whole of the interior of the nanocrystal has reorganized into an arrangement of six-membered rings. Comparing the final panel at 402 ps with the first at 0 ps, there appears to have been little change in the structure of the surface skin throughout the time taken for the interior to transform.

The same image as in the final frame of Fig. 4 is repeated in Fig. 5, rotated anticlockwise by 30°. The close-packed layers in the product lie horizontally on the right-hand side of the image, and the stacking sequence has been identified. There are two B3 regions separated by a single B4 region, which all have the same close-packed orientation, differing only in their local stacking sequence. The left-hand side of the figure is more difficult to assign, with six-membered boats and four-membered square rings visible.

Figure 6 shows the same nanocrystal at the same point in time, with a slice taken through the center from a slightly

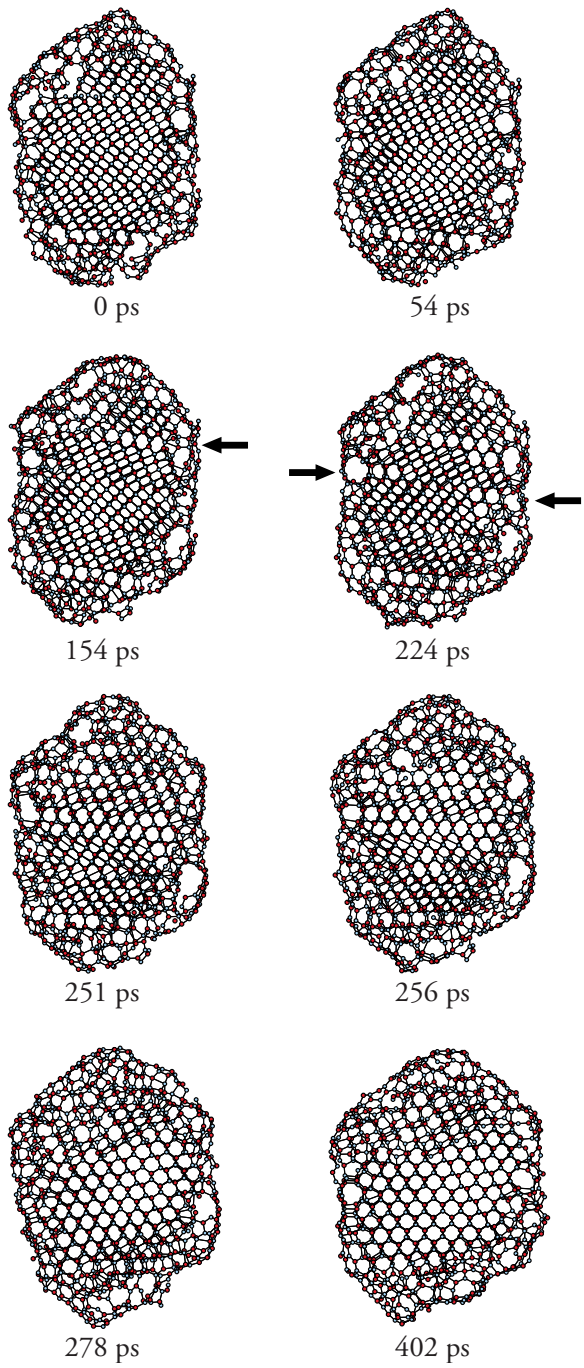

FIG. 4. (Color online) A series of molecular dynamics snapshots of a slice through the 3246 ion nanocrystal as it undergoes a B1 to four-coordinate transition. The initial view at 0 ps is along the B1 [110] direction, clearly showing the Σ_3 grain boundaries formed in the previous B3→B1 transition. The arrows in the third and fourth frames highlight regions of the crystal where there is a ring opening.

different orientation. The vertical axis of the nanocrystal has the same orientation as in Fig. 5, with a rotation of 60° made about it. Several different crystalline grains are seen. The three regions arranged one above another down the center of the slice are the same B3-B4-B3 section seen on the right-hand side of Fig. 5.

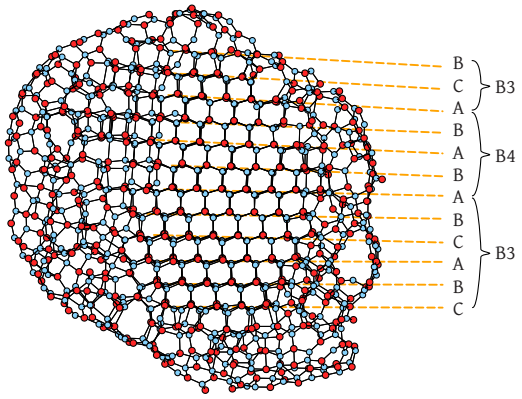

FIG. 5. (Color online) A slice through the 3246 ion nanocrystal showing the stacking sequence of the close-packed planes. This is the same configuration as shown in the final panel of Fig. 4 but has been rotated so that the close-packed layers lie close to horizontal. A single B4 and two B3 regions can be seen.

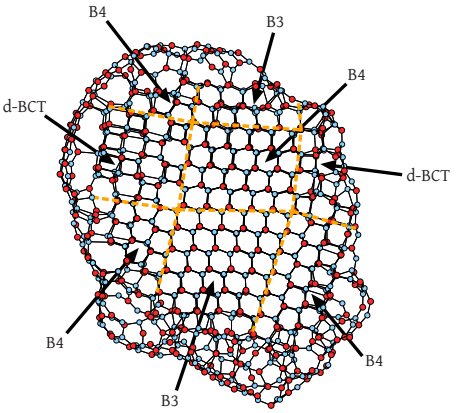

FIG. 6. (Color online) Another slice through the same nanocrystal shown in Figs. 4 and 5. This direction of view lies at a 60 ° angle to that in the previous figure, with the axis of rotation relating the two lying in the vertical plane of the page. From this perspective B3, B4, and d-BCT regions can be seen.

Either sides of the lower B3 region are two more B4 areas. They have their local *c* directions oriented differently from the B4 section in the center of the slice. This is possible because of the different arrangements of chairs and boats that gives rise to the difference in stacking sequences in the B3 and B4 structures. The B4 structure has chair conformations making up the close-packed *ab* plane, with boats in the *c* direction, whereas for B3 the entire structure is constructed from chairs, making the three crystallographic ⟨001⟩ directions locally equivalent. All three of these B4 regions have the same close-packed orientation as *one* of these three equivalent close-packed directions in the mutually neighboring B3 region. Tetrahedral coordination is possible without disruption for each of these three orientations, and all three B3-B4 boundaries are locally equivalent to stacking faults, as the differently oriented B4 regions do not come into direct contact.

On either sides of the central B4 region are two sections with a third crystal structure. These have been labeled as diatomic-body-centered tetragonal (d-BCT) since they share a structural motif with the BCT zeolite structure.[50,51] The ions are arranged with alternating anions and cations in positions that would be occupied by silicon atoms in the zeolite framework, and a single M-X bond here corresponds to a Si–O–Si fragment. Hamad and Catlow[47] have observed the d-BCT structure in simulated annealing of $ZnS_n (n \leq 512)$, and found it to be more stable than both B3 or B4 for these small clusters while Doll *et al.*[52] have predicted d-BCT as a low-energy metastable structure for LiF. Two-dimensional d-BCT regions have also been observed to spontaneously form in simulations of the relaxation of freshly-cleaved wurtzite nanocrystals, where they form an inversion domain boundary (IDB*) interface between regions with opposite $[0001]_{B4}$ orientations (Ref. 53), recently observed directly in transmission electron miscroscopy (TEM) images of ZnO films.[54] The formation of d-BCT regions is a consequence of the sequence of mechanistic events occurring during the transition, themselves a consequence of the geometry of the high-pressure starting structure.

The d-BCT structure is constructed from planes of boats arranged along two perpendicular directions with each boat arranged "back-on" to another, forming an array of four- and eight-membered rings when viewed along the local *c* direction, achieving near-tetrahedral local coordination. At a B4-d-BCT boundary, one of the d-BCT layers of boats is equivalent to a B4 plane lying parallel to the new close-packed direction. Since these layers of d-BCT layers exist with two perpendicular orientations, it is possible to form commensurate boundaries with B4 regions that have orientations related by a 90° rotation (as B3 can). Formation of d-BCT regions is likely to reduce the energy of the crystal compared with forming an interface between two mismatched B4 regions, even though the bulk energy of these in isolation would be lower than that of the d-BCT structure. In finite domains such as these, the polar nature of the B4 structure may require polar surfaces at domain edges leading to unfavorable domain-surface energy contributions.

C. Nucleation and growth

The observed formation of multiple regions with different structures contrasts with previous decompression simulations of single-domain wurtzite nanocrystals.[42] These nanocrystals had well-defined surfaces, and a B1→B4 transition proceeded via a single surface-nucleation event, with subsequent domain growth. Where there is a single nucleation event, with a single 2×3 unit opening to form a distorted hexagon, then it is relatively simple to see how this can then control the rest of the transformation, and an ideal single-domain structure results. Furthermore, the orientation of this first ring opening determines the orientation of the crystal lattice in the whole of the product structure. If, however, multiple nucleation events occur then there is no guarantee that all these ring openings are compatible with a final crystal structure with a uniform orientation, and this can lead to the formation of multigranular product nanocrystals.

For the nanocrystals described here, no surface nucleation is observed. The high pressure starting structures already have disordered four-coordinate surfaces. Instead nucleation occurs at the various Σ_3 grain boundaries throughout the B1

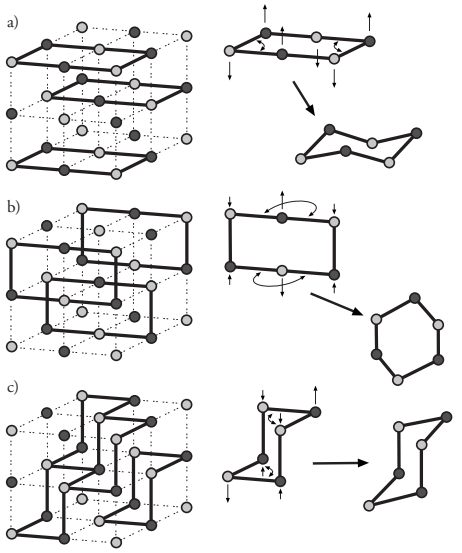

FIG. 7. Schematic representation of the rock-salt (B1) to zinc blende (B3) mechanism.

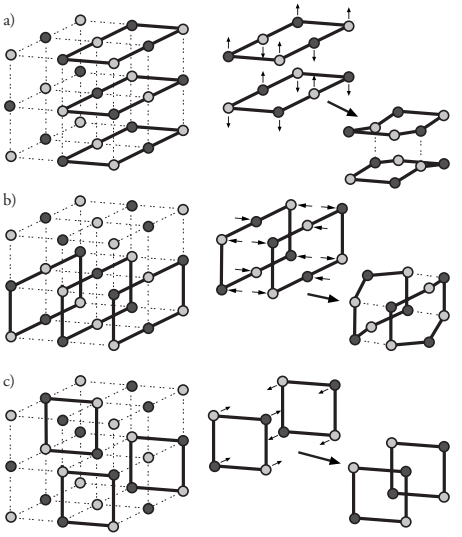

FIG. 8. Schematic representation of the B1 to d-BCT mechanism.

crystal. These grain boundaries are able to undergo a ring opening at a higher pressure than the rest of the structures because they are effectively stacking faults between the close-packed (111) layers of the B1 crystal. Whether B3 or B4 forms locally is likely to be determined by kinetic considerations, with particular geometries in the bounding disordered surface region favoring the close-packed layers moving in a particular direction in the $(111)_{B1}$ plane. Furthermore, in the case of a local B4 structure forming, this arrangement of anions will also decide the orientation of the local *c* direction, which will either form oriented perpendicular to the original plane of the Σ_3 grain boundary or oriented with a 60° relative rotation as is the case in the above example.

In the starting high-pressure structure, the Σ_3 grain boundaries are parallel. Thus the nucleation regions share a common close-packed orientation, and the final low-pressure structure is mostly a continuous B4/B3 region with stacking faults. B3 regions that do form during this process can then grow along any of the equivalent $\langle 111 \rangle$ directions to produce B4 regions with close-packed orientations perpendicular to the original Σ_3 planes, and the d-BCT structure forming when two differently oriented B4 regions come into contact to accommodate this lattice mismatch.

D. Local six- to four-coordinate mechanisms

Close examination of the trajectories allows the local mechanisms that produce the structures described above to be determined. The B3, B4, and d-BCT structures are characterized by different combinations and arrangements of six-membered chairs and boats, and the formation of all three can be described in a similar fashion. Three mechanisms are Peierls-type distortions that consist of opening up of B1 square nets with the arrangement of bond-breaking events determining the local structure in the product system, while the fourth mechanism is an alternative B1→B4 pathway, which involves bond formation in addition to bond breaking.

1. B1→B3

In the transformation from octahedral to tetrahedral coordination, the most basic unit that it is useful to consider is the 2×3 square nets that open to give the six-membered rings in the product crystal. It is the choice of conformations adopted by these six-membered rings, as well as their relative orientation in the product nanocrystal that determines the exact final structure. If all the rings open to form chairs, a B3 structure results. A schematic of the mechanism for this process is shown in Fig. 7. The middle two atoms of 2×3 rectangles lying in two perpendicular $(100)_{B1}$ planes pucker to form chairs, as shown in the panels [Figs. 7(a) and 7(b)]. This forms two of the three equivalent orientations of chairs that make up the product B3 structure. The third set of chairs are formed as shown in the panel [Fig. 7(c)]: $(111)_{B1}$ layers slide apart and the cations move to occupy the tetrahedral holes in the newly formed lattice. This mechanism is the same as that proposed by Wickham *et al.*[45] in order to be consistent with the observation that the long $[111]_{B3}$ axis of mixed B3/B4 CdSe nanocrystals transforms into a $[111]_{B1}$ direction on the application of pressure, and is equivalent to the bilayer sliding mechanism identified by Hatch *et al.*[40]

2. B1→d-BCT

If instead of only chairs being formed, some of the 2×3 rectangles open up to produce boats, then either the d-BCT or B4 structures will result. In the d-BCT structure, there are no chairs present. The 2×3 square nets lying in two perpendicular $(001)_{B1}$ planes open into boats, producing four- and eight-membered rings in the mutually perpendicular plane. A schematic of this process is shown in Fig. 8.

3. B1→B4

The case of the B1→B4 transition is more complicated as there are two mechanisms operating, the choice of which

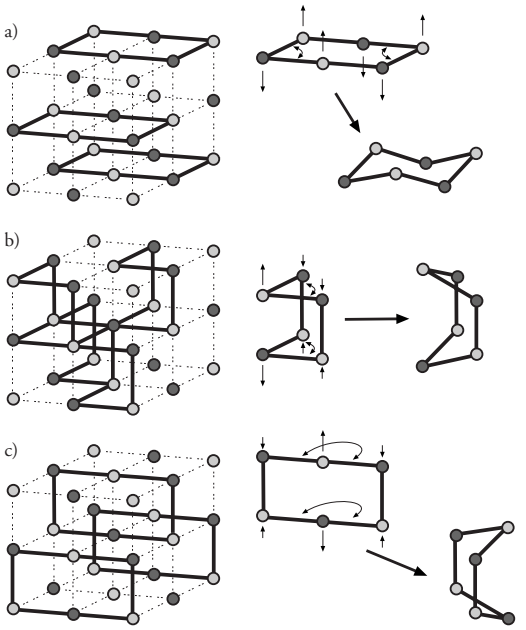

FIG. 9. Schematic representation of the B1→wurtzite (B4) mechanism I (Ref. 42).

is locally adopted determining the relationship between the initial and the final crystal orientations. There are multiple grains in the starting B1 structure, with local $[001]_{B1}$ directions which differ by 60° as a consequence of the formation of the Σ_3 grain boundaries during the forward transition.[37] In the B1→B4 mechanism observed in previous nanocrystal downstroke simulations,[42] the $[001]_{B1}$ direction transformed into the $[0001]_{B4}$ since it is this plane that opens up to give the layers of chairs in the product structure (Fig. 9). If this mechanism occurred in all the regions undergoing a B1→B4 transition in the crystal modeled here, it might be expected that the initial difference in lattice tilts would also be observable in the low-pressure product. However, this is not the case, and differently aligned neighboring B1 regions are able to transform into a coherent B4 region with a single close-packed orientation.

This is illustrated in Fig. 10, which has been taken from a different decompression trajectory. This shows a section of the interior of a nanocrystal with two differently oriented B1 regions meeting at a Σ_3 grain boundary. The first panel shows the grain boundary running vertically down the image. To the left of the grain boundary, ions of the same color all lie in the same $(001)_{B1}$ plane, indicating a region that transforms via the $[001]_{B1} \rightarrow [0001]_{B4}$ mechanism seen in previous simulations,[29] and which will be denoted as mechanism I. In the right-hand region, however, cations and anions make offset pairs of $(111)_{B1}$ planes that transform via a $[111]_{B1} \rightarrow [0001]_{B4}$ mechanism, which will be denoted as mechanism II. Pairs of $(111)_{B1}$ planes already define layers of distorted chairs, which can open up to form the chairs in the close-packed planes of the product. In the B1→B3 mechanism all of the $(111)_{B1}$ planes open up in the same way, since the chairs in the product structure all have the same orientation. In the B4 structure, however, the orientation of these chairs inverts on going from layer to layer, which is inconsistent with a Peierls-type ring opening. Instead half of the paired layers open up in the same way as in the B1→B3 mechanism, while for the other half, the changes in bond connectivity are different in order to produce these inverted chairs. Figure 11 shows the ions in the B1 structure, which then form individual chairs, as well as the motions required for the transformation.

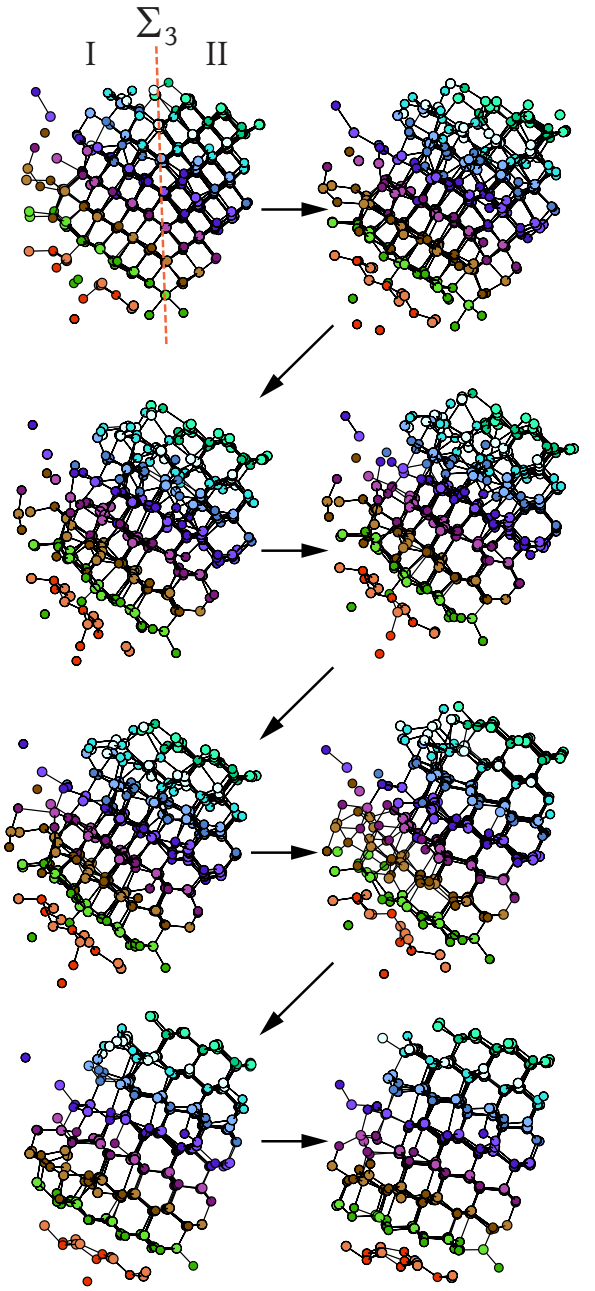

FIG. 10. (Color online) A sequence of molecular dynamics snapshots showing a region undergoing a B1 to B4 transition. The ions are colored according to the close-packed layer they sit in at the final structure. In each individual layer, the cations are shaded to be darker than the anions.

The long-ranged relationship between these different $(111)_{B1}$ layers can be seen in Fig. 12, which shows the alternating planes according to which of the two mechanisms they transform by, or equivalently according to the orienta-

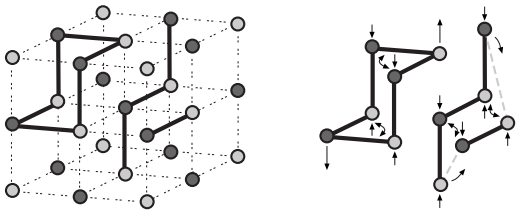

FIG. 11. Schematic of the B1→B4 mechanism II showing the motions undergone to produce oppositely oriented chairs in what become the $(0001)_{B1}$ close-packed planes.

tion of the chairs formed in the product structure. The B1→B4 mechanism II can alternatively be viewed as a combination of a B1→B3 ring opening along the $(111)_{B1}$ planes, and the sliding of these (111) planes in alternating directions. Such a sliding of close-packed planes between B3 and B4 phases (albeit in the reverse direction to that seen here) has recently been seen in GaAs nanowires, where a B4→B3 transition is induced by epitaxial burying.[55]

Because different B1 grains through a B1 nanocrystal can all transform via alternating mechanisms, i.e., mechanism I-II-I-II, then it is possible for the entire product nanocrystal to have close-packed planes with the same orientation, appearing as a single region, although it will most likely still contain stacking faults. However, this outcome is not guaranteed, and it is possible to have adjacent B1 regions that transform via the same mechanism, e.g., II–I–I–II. Figure 13 shows a slice through a product nanocrystal where this is the case, resulting in two four-coordinate regions, both of which display stacking faults, that have close-packed orientations which differ by 60°. It is likely that this variation is determined by a tradeoff between the lower local barrier if the $B1 \xrightarrow{I} B4$ mechanism is followed, and the energetic penalty involved in forming this grain boundary in the product structure. There is also likely to be an effect due to the relative differences in changes of energy in the surface region, since the two mechanisms require different distortions to the nanocrystal shape. The 60° domain boundary is made possible by the presence of five-coordinate cations.

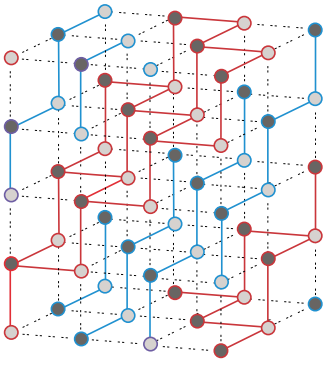

FIG. 12. (Color online) Schematic showing the alternating close-packed $[111]_{B1}$ layers, colored according to which local mechanism they transform by. The red ions are those that transform in the same way as for the B1→B3 mechanism, whereas those in blue rearrange according to the alternative mechanism. In both cases the colored bonds indicate those that remain unbroken throughout the transition.

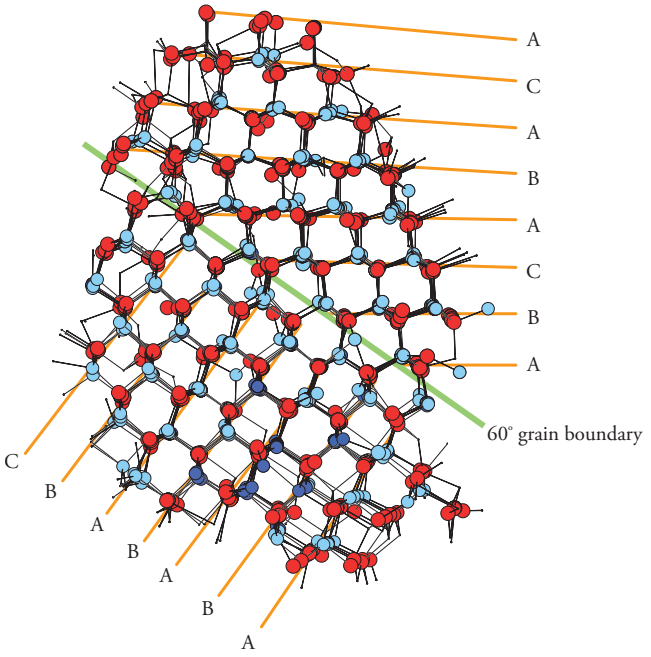

FIG. 13. (Color online) A slice through the center of another 3246 ion nanocrystal after a B3→B1→B3/B4 cycle. Only ions that were octahedrally coordinated in the high-pressure B1 phase are shown. Two distinct regions can be seen with different orientations of their close-packed layers.

IV. SUMMARY

Using constant-pressure molecular dynamics, particles that have previously undergone B3→B1 transitions have been shown to convert back to four-coordinate structures when the applied pressure is decreased. The reverse transition is observed at a pressure of 2.3 GPa, indicating considerable hysteresis. The midpoint of the forward and reverse transition pressures is 5.65 GPa. This is slightly above the thermodynamically predicted B3↔B1 transition pressure of 5.2 GPa, in agreement with the increase in the transition pressure observed experimentally as particle sizes are reduced.[56] However, since the mechanistic processes observed in the downstroke transition are very different to those in the upstroke simulations, there may be very different kinetic barriers for each process. If this is the case, it would mean an assumption of a symmetric hysteresis loop with a zero-width limiting point at its center would not be valid.

The behavior contrasts with B4→B1→B4 behavior observed in previous simulations[29,42] since the product four-coordinate particles are very different to the initial B3 crystals. The high-pressure nanocrystals formed during the B3→B1 transitions have disordered surfaces and also display grain boundaries. Since the surface is already relatively low in energy, nucleation instead occurs internally at the Σ_3 boundaries. The high-pressure crystals have several of these grain boundaries, and so multiple nucleation events are observed. Tetrahedrally coordinated regions grow from each of these, and complex structures are formed. There are a variety of observed local mechanisms. B4 regions form via the same mechanism as seen previously,[42] and B3 regions form through a related mechanism. In both cases, a $[001]_{B1}$ direc-

tion becomes the close-packed direction in the product structure. Because of the similarities between these two mechanisms, stacking faults and B3–B4 grain boundaries form readily in these four-coordinate regions. The formation of the non-close-packed d-BCT structure is also observed, which appears when two B4 regions with different close-packed orientations grow into one another. The B3 structure is less stable for the interatomic potential used here but may become accessible at a higher pressure than the B4; therefore forming under kinetic control. The presence of the grain boundaries in the high-pressure starting structures is responsible for further complications. The B1 regions on either sides of these boundaries have different orientations, and in order to form continuous B4 regions, a second $B1 \rightarrow B4$ mechanism is adopted in which the $[111]_{B1}$ direction transforms into the $[0001]_{B4}$. The observed $B1 \rightarrow B3$ and $B1 \overset{II}{\rightarrow} B4$ mechanisms are both consistent with the observations of Wickham *et al.*, where there was a correspondence between the $[0001]_{B4}/[111]_{B3}$ and $[111]_{B1}$ directions.[45]

ACKNOWLEDGMENT

This work was supported by EPSRC Grant No. GR/R57584/01.

*morganb@tcd.ie

[1] A. L. Edwards and H. G. Drickamer, Phys. Rev. **122**, 1149 (1961).
[2] X.-S. Zhao, J. Schroeder, T. G. Bilodeau, and L.-G. Hwa, Phys. Rev. B **40**, 1257 (1989).
[3] J. R. Chelikowsky and J. K. Burdett, Phys. Rev. Lett. **56**, 961 (1986).
[4] J. R. Chelikowsky, Phys. Rev. B **34**, 5295 (1986).
[5] F. Decremps, J. Pellicer–Porres, F. Datchi, J. P. Itié, A. Polian, F. Baudelet, and J. Z. Jiang, Appl. Phys. Lett. **81**, 4820 (2002).
[6] S. H. Tolbert and A. P. Alivisatos, J. Chem. Phys. **102**, 4642 (1995).
[7] S. H. Tolbert and A. P. Alivisatos, Annu. Rev. Phys. Chem. **46**, 595 (1995).
[8] A. P. Alivisatos, J. Phys. Chem. **100**, 13226 (1996).
[9] T. Vossmeyer, L. Katsikas, M. Giersig, I. G. Popovic, and H. Weller, J. Phys. Chem. **98**, 7665 (1994).
[10] H. Zhang, B. Gilbert, F. Huang, and J. F. Banfield, Nature (London) **424**, 1025 (2003).
[11] B. Gilbert, H. Zhang, F. Huang, and J. F. Banfield, J. Chem. Phys. **120**, 11785 (2004).
[12] A. S. Barnard and L. A. Curtiss, Nano Lett. **5**, 1261 (2005).
[13] M. Wilson and P. A. Madden, J. Phys.: Condens. Matter **14**, 4629 (2002).
[14] F. Shimojo, S. Kodiyalam, I. Ebbsjō, R. K. Kalia, A. Nakano, and P. Vashishta, Phys. Rev. B **70**, 184111 (2004).
[15] D. Zahn, Y. Grin, and S. Leoni, Phys. Rev. B **72**, 064110 (2005).
[16] G. J. Ackland, Phys. Status Solidi B **223**, 361 (2001).
[17] A. Nazzal and A. Qteish, Phys. Rev. B **53**, 8262 (1996).
[18] N. E. Christensen, D. L. Novikov, R. E. Alonso, and C. O. Rodriguez, Phys. Status Solidi B **211**, 5 (1999).
[19] A. Zunger, K. Kim, and V. Ozalines, Phys. Status Solidi B **223**, 369 (2001).
[20] M. A. Blanco, J. M. Recio, A. Costales, and P. Ravindra, Phys. Rev. B **62**, R10599 (2000).
[21] S. Limpijumnong and S. Jungthawan, Phys. Rev. B **70**, 054104 (2004).
[22] J. K. Burdett and T. J. McLarnan, J. Chem. Phys. **75**, 5764 (1981).
[23] J. K. Burdett, Prog. Solid State Chem. **15**, 173 (1984).
[24] A. M. Saitta and F. Decremps, Phys. Rev. B **70**, 035214 (2004).
[25] M. D. Knudson, Y. M. Gupta, and A. B. Kunz, Phys. Rev. B **59**, 11704 (1999).
[26] H. Sowa, Solid State Sci. **7**, 73 (2005).
[27] H. T. Stokes, J. Gunter, D. M. Hatch, J. Dong, H. Wang, and J. P. Lewis, Phys. Rev. B **76**, 012102 (2007).
[28] X. Ye, D. Y. Sun, and X. G. Gong, Phys. Rev. B **77**, 094108 (2008).
[29] B. J. Morgan and P. A. Madden, Phys. Chem. Chem. Phys. **8**, 3304 (2006).
[30] M. Grünwald, E. Rabani, and C. Dellago, Phys. Rev. Lett. **96**, 255701 (2006).
[31] M. Grünwald, C. Dellago, and P. L. Geissler, J. Chem. Phys. **127**, 154718 (2007).
[32] M. Grünwald and C. Dellago, Mol. Phys. **104**, 3709 (2006).
[33] N. J. Lee, R. K. Kalia, A. Nakano, and P. Vashishta, Appl. Phys. Lett. **89**, 093101 (2006).
[34] F. Shimojo, I. Ebbsjö, R. K. Kalia, A. Nakano, J. P. Rino, and P. Vashishta, Phys. Rev. Lett. **84**, 3338 (2000).
[35] M. Wilson, F. Hutchinson, and P. A. Madden, Phys. Rev. B **65**, 094109 (2002).
[36] S. Kodiyalam, R. K. Kalia, H. Kikuchi, A. Nakano, F. Shimijo, and P. Vashishta, Phys. Rev. Lett. **86**, 55 (2001).
[37] B. J. Morgan and P. A. Madden, Nano Lett. **4**, 1581 (2004).
[38] S. Kodiyalam, R. K. Kalia, A. Nakano, and P. Vashishta, Phys. Rev. Lett. **93**, 203401 (2004).
[39] M. S. Miao and W. R. L. Lambrecht, Phys. Rev. Lett. **94**, 225501 (2005).
[40] D. M. Hatch, H. T. Stokes, J. Dong, J. Gunter, H. Wang, and J. P. Lewis, Phys. Rev. B **71**, 184109 (2005).
[41] K. Jacobs, D. Zaziski, E. C. Scher, A. B. Herhold, and A. P. Alivisatos, Science **293**, 1803 (2001).
[42] B. J. Morgan and P. A. Madden, J. Phys. Chem. C **9**, 2355 (2007).
[43] M. P. Finnegan, H. Zhang, and J. F. Banfield, J. Phys. Chem. C **111**, 1962 (2007).
[44] C. M. Goodell, B. Gilbert, S. J. Weigand, and J. F. Banfield, J. Phys. Chem. C **112**, 4791 (2008).
[45] J. N. Wickham, A. B. Herhold, and A. P. Alivisatos, Phys. Rev. Lett. **84**, 923 (2000).
[46] Y.-G. Guo, J.-S. Lee, Y.-S. Hu, and J. Maier, J. Electrochem. Soc. **154**, K51 (2007).
[47] S. Hamad and C. R. A. Catlow, J. Cryst. Growth **294**, 2 (2006).
[48] S. Hamad, C. R. A. Catlow, S. M. Woodley, S. Lago, and J. A. Mejías, J. Phys. Chem. B **109**, 15741 (2005).
[49] G. J. Martyna, D. J. Tobias, and M. L. Klein, J. Chem. Phys.

101, 4177 (1994).
[50] W. A. Dollase and C. R. Ross II, Am. Mineral. **78**, 627 (1993).
[51] The Database of the Structure Commission of the International Zeolite Association, http://www.iza-structure.org/databases/
[52] K. Doll, J. C. Schön, and M. Jansen, Phys. Chem. Chem. Phys. **9**, 6128 (2007).
[53] B. J. Morgan and P. A. Madden, Phys. Chem. Chem. Phys. **9**, 2355 (2007).
[54] Y. Z. Liu, H. T. Yuan, Z. Q. Zeng, X. L. Du, X. D. Han, Q. K. Xue, and Z. Zhang, Philos. Mag. Lett. **87**, 687 (2007).
[55] G. Patriarche, F. Glas, M. Tchernycheva, C. Sartel, L. Largeau, J.-C. Harmand, and G. E. Cirlin, Nano Lett. **8**, 1638 (2008).
[56] K. Jacobs, J. Wickham, and A. P. Alivisatos, J. Phys. Chem. B **106**, 3759 (2002).